

# Light dark matter searches with positrons

Marco Battaglieri<sup>1,3</sup>, Mariangela Bondi<sup>1</sup>, Andrea Celentano<sup>1</sup>, Marzio De Napoli<sup>2</sup>, and Luca Marsicano<sup>1</sup>

<sup>1</sup>Istituto Nazionale di Fisica Nucleare, Sezione di Genova, 16146 Genova, Italia

<sup>2</sup>Istituto Nazionale di Fisica Nucleare, Sezione di Catania, 95125 Catania, Italia

<sup>3</sup>JLab

**We present two complementary measurements to search for light dark matter at Jefferson Laboratory, exploiting a possible positron beam available in the future at this facility. Light dark matter is the new compelling hypothesis that identifies dark matter with new sub-GeV “Hidden Sector” states, neutral under Standard Model interactions and interacting with our world through a new force. Accelerator-based searches at the intensity frontier are uniquely suited to explore it.**

**Thanks to the unique properties of the CEBAF (Continuous Electron Beam Accelerator Facility) beam – the high intensity and the high energy – and exploiting a novel light dark matter production mechanism, the positron annihilation on atomic electrons, the proposed experiments will be able to explore new regions in the light dark matter parameters space, confirming or ruling out this hypothesis.**

## Introduction

The existence of dark matter (DM) is a “smoking gun” evidence of physics beyond the Standard Model (SM). However, all experimental evidence is based on gravitational effects, and **so far we know nothing about the particle content of DM: uncovering this puzzle is thus a top priority in fundamental physics.** Since its formulation, this compelling question motivated a large number of experiments aimed at DM detection. So far the theoretical and experimental efforts have focused on the WIMPs (Weakly Interacting Massive Particles) scenario, assuming new high mass particles interacting via the known SM weak force (1). However, null results in direct detection experiments of galactic halo DM and in high-energy accelerator searches at the LHC call for an alternative explanation to the current paradigm (2).

In recent years a new, alternative hypothesis for the DM nature has been introduced. This predicts the existence of sub-GeV **light dark matter** (LDM) particles, interacting with SM states through a new interaction. The simplest model predicts LDM particles (denoted as  $\chi$ ) with masses below  $1 \text{ GeV}/c^2$ , charged under a new force and interacting with the SM particles via the exchange of a light spin-1 boson, usually referred to as “heavy photon” or “dark photon” ( $A'$ ) (3–5). This picture allows the existence of an entire new “Dark Sector”, with its own particles and interactions, and is compatible with the well-motivated hypothesis of DM thermal origin (6). It assumes that, in the early Universe, DM reached the thermal equilibrium with SM particles through an interaction mechanism such as the one described above. The present DM density, deduced from astrophysics measurements, is thus a relic “remnant” of its primordial abundance (6). The thermal origin hypothesis provides a relation between the observed DM density and the model parameters, resulting in a

clear, predictive target for discovery or falsification (7).

Many LDM models have been proposed, with different hypothesis for the LDM to  $A'$  coupling (diagonal or off-diagonal), as well as for the particle nature (scalar or fermion). However, the phenomenology of thermal freeze-out and the consequences on the LDM particle physics model arise solely from the ratio between the mediator and the LDM mass. In particular, the most relevant scenario for accelerator-based experiments is the *direct annihilation regime* in which  $2m_\chi < m_{A'}$ . In this case, the dominant LDM-to-SM process is the  $s$ -channel virtual mediator exchange,  $\chi\bar{\chi} \rightarrow A'^* \rightarrow f\bar{f}$ , where  $f$  is a charged SM fermion. The velocity-averaged cross-section for this process scales as  $\langle\sigma v\rangle \simeq \alpha_D \varepsilon^2 m_\chi^2 / m_{A'}^4$ , with the  $\chi$ -to- $A'$  mass ratio and the dark coupling  $g_D = \frac{\alpha_D}{4\pi}$  at most  $\mathcal{O}(1)$  and the parameter  $\varepsilon$  defining the intensity of the mixing between the dark photon and the SM photon.

Since the thermal origin mechanisms implies  $\Omega_{\text{DM}} \propto 1/\langle\sigma v\rangle$ , the *minimum* SM-LDM coupling compatible with the observed DM abundance is:  $\Omega_{\text{DM}} = 0.269 \pm 0.007$  (8):

$$y \equiv \varepsilon^2 \alpha_D \left( \frac{m_\chi}{m_{A'}} \right)^4 \gtrsim \langle\sigma v\rangle_{\text{relic}} m_\chi^2. \quad (1)$$

This constraint, within the simple  $A'$  model, is valid for every DM/mediator variation up to order-one factors, provided that  $m_{\text{DM}} < m_{\text{MED}}$ : **reaching this benchmark sensitivity is the ultimate goal of all light dark matter searches.**

## Dark sector searches with positron beams on fixed targets

The production of LDM particles can be generated in collisions of electrons or positrons of several GeV with a fixed target by the processes depicted in Fig. 1, with the final state  $A'$  decaying to a  $\chi\bar{\chi}$  pair. For experiments with electron beams, diagram (a), analogous to ordinary photon bremsstrahlung, is the dominant process, although it was recently shown that for thick-target setups, where positrons are generated as secondaries from the developing electromagnetic shower, diagrams (b) and (c) give non-negligible contributions for selected regions of the parameters space (9) – See Ref. (7) for a comprehensive review of past/current experiments and future proposals.

On the other hand, for experiments with positron beams, diagrams (b) and (c) play the most important role. In this document, we present two complementary measurements to search for light dark matter with positron beams at Jefferson Laboratory, exploiting the unique potential of the proposed

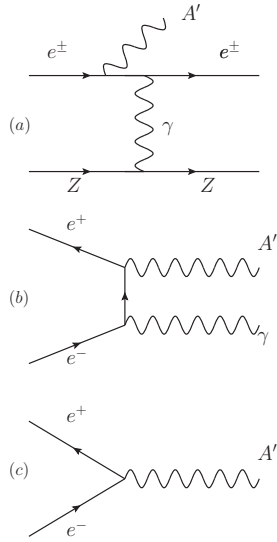


**Fig. 1.** Three different  $A'$  production modes in fixed target lepton beam experiments: (a)  $A'$ -strahlung in  $e^-/e^+$ -nucleon scattering; (b)  $A'$ -strahlung in  $e^+e^-$  annihilation; (c) resonant  $A'$  production in  $e^+e^-$  annihilation.

$e^+$ -beam facility. In the following, we introduce the two approaches, and for each one we briefly discuss the experimental setup, the measurement strategy, the data analysis, and the foreseen results. We underline that Jefferson Laboratory is playing a leading role in the LDM searches, with different experiments already running, HPS (10) and APEX (11), or approved to run in the near future, BDX (12) and Dark-Light (13).

**1. Thin-target measurement.** This measurement exploits the  $A'$ -strahlung production in electron-positron annihilation described by diagram (b). The primary positron beam impinges on a thin target, where a photon- $A'$  is produced. By detecting the final-state photon in an electromagnetic calorimeter, the missing mass kinematic variable  $M_{miss}$  can be computed event-by-event:

$$M_{miss}^2 = (P_{beam} + P_{target} - P_{\gamma})^2. \quad (2)$$

The signal would show up as a peak in the missing mass distribution, centered at the  $A'$  mass, on top of a smooth background due to SM processes resulting from events with a single photon measured in the calorimeter. The peak width is mainly determined by the energy and angular resolution of the calorimeter. Several experiments searching for  $A'$  with this approach have been proposed. PADME (Positron Annihilation into Dark Matter Experiment) at LNF (14) is one of the first  $e^+$  on thin target experiment searching for  $A'$ . It uses the 550 MeV positron beam provided by the  $DA\Phi NE$  linac at INFN LNF (Laboratori Nazionali di Frascati) impinging on a thin diamond target.

**2. Active thick-target measurement.** This measurement exploits the resonant  $A'$  production by positrons annihilation on atomic electrons described by diagram (c). The primary positron beam impinges on a thick active target, and the missing energy signature of produced and undetected  $\chi$

is used to identify the signal (15). The active target measures the energy deposited by the individual beam particles: when an energetic  $A'$  is produced, its invisible decay products – the  $\chi\bar{\chi}$  pair – will carry away a significant fraction of the primary beam energy, thus resulting in measurable reduction in the expected deposited energy. Signal events are identified when the missing energy  $E_{miss}$ , defined as the difference between the beam energy and the detected energy, exceeds a minimum threshold value. The signal has a very distinct dependence on the missing energy through the relation<sup>1</sup>  $m_{A'} = \sqrt{2m_e E_{miss}}$ . This results in a specific experimental signature for the signal, that would appear as a peak in the missing energy distribution, at a value depending solely on the dark photon mass. Thanks to the emission of soft Bremsstrahlung photons, the thick target provides an almost continuous energy loss for the impinging positrons. Even though the positron energy loss is a quantized process, the finite intrinsic width of the dark photon – much larger than the positron energies differences – and the electrons energy and momentum spread induced by atomic motions (16) will indeed compensate this effect. This allows the primary beam to “scan” the full range of dark photon masses from the maximum value (corresponding to the loss of all the beam energy), to the minimum value fixed by the missing energy threshold (17), exploiting the presence of secondary positrons produced by the developing electromagnetic shower.

## 1. Positron annihilation on a thin target

**Signal signature and yield.** The differential cross-section for dark photon production via the positron annihilation on the atomic electron of the target  $e^+e^- \rightarrow A'\gamma$ , is given by:

$$\frac{d\sigma}{dz} = \frac{4\pi\alpha^2\epsilon^2}{s} \left( \frac{s - m_{A'}^2}{2s} \frac{1 + z^2}{1 - \beta^2 z^2} + \frac{m_{A'}^2}{s - m_{A'}^2} \frac{1}{1 - \beta^2 z^2} \right).$$

Here  $s$  is the  $e^+e^-$  system invariant mass squared,  $z$  is the cosine of the  $A'$  emission angle in the CM frame, measured with respect to the positron beam axis, and  $\beta = \sqrt{1 - \frac{4m_e^2}{s}}$ . This result has been derived at tree level, keeping the leading  $m_e$  dependence to avoid non-physical divergences when  $|z| \rightarrow 1$ . The emission of the annihilation products in the CM frame is concentrated in the  $e^+e^-$  direction. This results in an angular distribution for the emitted  $\gamma$  peaked in the forward direction in the laboratory frame. In the case of invisible decays, the  $A'$  escapes detection, while the  $\gamma$  can be detected in the downstream electromagnetic calorimeter (ECAL). The measurement of the photon energy and emission angle, together with the precise knowledge of the primary positron momentum, allows computing the missing mass kinematic variable from Eq. 2. The mass range that can be spanned is constrained by the available energy in the center of mass frame: using an 11 GeV positron beam at JLab,  $A'$  masses up to  $\sim 106 \text{ MeV}/c^2$  can be explored.

The signal yield has been evaluated using CALCHEP (18); the widths  $\sigma(m_{A'})$  of the missing mass distributions of the

<sup>1</sup> $m_{A'}$  is the dark photon mass and  $m_e = 0.511 \text{ MeV}/c^2$  is the electron mass.

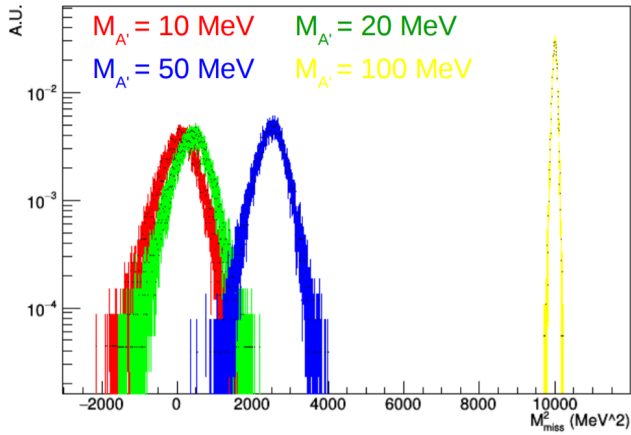


Fig. 2. Computed missing mass spectrum for signal events for 4 different values of  $m_{A'}$ .

measured recoil photon has been computed for six different values of the  $A'$  mass value in the 1–103 MeV range. CALCHEP provides the total cross section of the process, for  $\varepsilon = 1$ ; the cross section value as a function of  $\varepsilon$  has been obtained multiplying it by  $\varepsilon^2$ . Figure 2 shows results for 4 mass values: due to the  $e^+e^- \rightarrow \gamma A'$  process kinematics, the missing mass resolution for the signal is best for large  $A'$  masses and degraded for a “light”  $A'$  ( $m_{A'} < 50$  MeV).

**Expected background.** All processes resulting in a single  $\gamma$  hitting the calorimeter represent the background for the experiment, the most relevant being *bremsstrahlung* and the  $e^+e^-$  annihilation processes in two and three photons. In order to reduce the bremsstrahlung background, the proposed detector features an active veto system composed of plastic scintillating bars: positrons losing energy via bremsstrahlung in the target are detected in the vetos, rejecting the event. However the high bremsstrahlung rate is an issue for this class of experiments, limiting the maximum viable beam current. To evaluate this background, a full GEANT4 (19) simulation of the positron beam impinging on the target has been performed. For all bremsstrahlung photons reaching the ECAL, the missing mass has been computed, accounting for the assumed detector angular and momentum resolution.

The  $e^+e^- \rightarrow \gamma\gamma$  and  $e^+e^- \rightarrow \gamma\gamma\gamma$  annihilation processes can produce background events whenever only one of the produced photons is detected in the ECAL. This contribution to background has been calculated as follows. Events have been generated directly using CALCHEP, which provided also the total cross sections for the processes. As in the case of bremsstrahlung, the missing mass spectrum was computed for events with a single photon hit in the ECAL. This study proved that, if one requires the measured energy to be greater than 600 MeV, the two photon annihilation background becomes negligible. This is due to momentum conservation: asking for only one photon to fall within the ECAL geometrical acceptance translates in a strong constraint on its energy. This argument does not apply to the three photon annihilation: this process generates an irreducible background for the experiment (see Fig. 3 for the missing mass spectrum

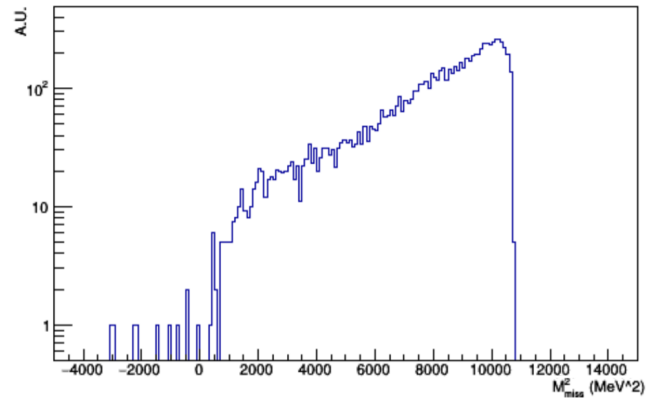


Fig. 3. Computed missing mass spectrum from positron annihilation into three photons events.

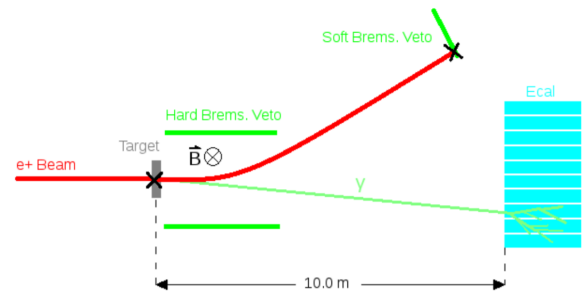


Fig. 4. Layout of the proposed thin target setup.

produced by the three-photon annihilation).

**Experimental Setup.** The experimental setup of the proposed measurement is shown in Fig. 4. The 11 GeV positron beam impinges on a  $100 \mu\text{m}$  thick carbon target, this material being a good compromise between density and a low  $Z/A$  ratio allowing to reduce bremsstrahlung rate. A magnet capable of generating a field of 1 T over a region of 2 m downstream the target bends the charged particles (including non-interacting positrons) away from the ECAL, placed a few meters downstream. The ECAL is composed of high density scintillating crystals, arranged in a cylindrical shape. High segmentation is necessary to obtain a good angular resolution, critical for a precise missing mass computation, but should however be matched with the Molière radius of the chosen material.

Crystals of  $\text{PbWO}_4$ ,  $\text{LSO}(\text{Ce})$  and  $\text{BGO}$ , represent optimal choices, given the fast scintillating time, high-density and short radiation length. Energy resolution, as well as angular resolution, plays a crucial role in the missing mass computation; a value of  $\frac{\sigma(E)}{E} = \frac{2\%}{\sqrt{E}}$  has been assumed for this study, consistent with the performance of the 23 cm long PADME BGO detector, corresponding to 20 radiation lengths. Such a depth is indeed needed for achieving this performance, due to longitudinal shower containment.

Since the small-angle bremsstrahlung high rate would blind the central crystals of the calorimeter, the simplest solution is to foresee a hole at the center of the cylinder. Assuming a radius of 30 cm and a distance from the target of 6 m, a geometrical acceptance of  $\sim 50$  mrad is achieved. In PADME,

with a crystal front-face of  $20 \times 20 \text{ mm}^2$ , a spatial resolution of  $\sim 3.5 \text{ mm}$  has been measured (significantly better than  $20 \text{ mm} / \sqrt{12}$ ). At 6 m distance this corresponds to an angular resolution of  $0.5 \text{ mrad}$ .

Besides the ECAL, the experimental setup includes a veto system to reduce the bremsstrahlung background. Following the layout of the PADME experiment, the vetos are composed of plastic scintillator bars. Whenever the primary  $e^+$  loses energy via bremsstrahlung in the target, its trajectory is bent by the magnetic field and it impinges on the veto bars, rejecting the event. For the sake of this study, a 99.5% veto efficiency has been considered. This assumption is proven realistic by the performance of the existing PADME experiment veto system (14).

Further suppression of the background can be achieved by placing a photon detector, much faster than the main calorimeter, covering its central hole. Such a fast calorimeter would also help in the reduction of  $\gamma\gamma$  and  $3\gamma$  events with one or two photons lost. In the case of PADME a  $5 \times 5$  matrix of  $3 \times 3 \text{ cm}^2$   $\text{PbF}_2$  crystals is used. The Cherenkov light from showers is readout by fast photo-multipliers, providing a  $\sim 2 \text{ ns}$  double pulse separation (to be compared with  $\sim 300 \text{ ns}$  decay time of the BGO).

**Positron beam requirements.** As already mentioned, the  $A'$  mass range that the proposed thin target experiment can explore is strictly constrained by the available energy in the center of mass frame. In this respect, a 11 GeV positron beam would allow extending significantly the  $A'$  mass range with respect to other similar experiments, up to  $\sim 106 \text{ MeV}/c^2$ . Being the  $e^+e^- \rightarrow \gamma A'$  annihilation a rare process, the sensitivity of the proposed search depends on the number of positron on target (POT) collected. In this setup, the maximum current is constrained by the bremsstrahlung rate on the ECAL innermost crystals. Therefore, a continuous beam structure is preferable. In this study, a continuous  $100 \text{ nA}$  beam has been considered, resulting in a manageable  $\sim 200 \text{ KHz}$  rate per crystal in the inner ECAL. In this configuration,  $10^{19}$  POT can be collected in 180 days, covering a new region in the  $A'$  parameter space. In the event that the available beam current is lower than  $100 \text{ nA}$ , a similar result can be obtained increasing the target thickness, at the price of a higher background due to multiple scattering.

The computation of the missing mass requires a precise knowledge of the primary positron momentum; this translates to certain requirements in terms of the quality of the beam. Here, a energy dispersion  $\frac{\sigma_{E_{Beam}}}{E_{Beam}} < 1\%$  and an angular dispersion  $\theta_{Beam} < 0.1 \text{ mrad}$  of the beam have been considered. With these assumptions, the missing mass resolution is dominated by the ECAL performance, with a negligible contribution from the beam dispersion.

**Reuse of the PADME components.** It's also interesting to investigate the possibility of reusing the existing PADME experimental apparatus as the starting point for the new thin target experiment at the CEBAF accelerator. In this paper we try to shortly review which part of the apparatus could

be directly reused, and which will need to be adapted to the different beam conditions.

The PADME target can be easily transferred and installed in the CEBAF accelerator, while the option of a ticker target will simplify the design and its easily achievable.

The PADME electromagnetic calorimeter performance is adequate with the requirements for the thin target experiment: in addition to the excellent energy resolution,  $< 2\% \sqrt{E}$ , and spatial resolution,  $\sim 3.5 \text{ mm}$ , single BGO crystals are capable of tolerating rates in excess of  $2 \text{ MHz}$ . The increased energy of the beam from 0.5 to 11 GeV would improve the energy resolution, but will also enhance the contribution of longitudinal shower containment to the resolution with respect to the stochastic term. The overall effect should not degrade the resolution significantly, due to the sufficient total depth of  $\sim 20 X_0$ .

The small angle calorimeter will also profit by the much higher energy of the impinging photons, but will suffer more the longitudinal leakage, being only  $15 X_0$  long. This will not compromise its use as photon veto, while performance as calorimeter, for improving  $2\gamma$  and  $3\gamma$  acceptance, needs to be evaluated.

The charged veto system will certainly require a different geometrical assembly, both due to the need of a longer magnet and the different boost, but the technology and front-end electronics can be reused.

The trigger and DAQ system of the PADME experiment was built to operate at a rate of  $50 \text{ Hz}$  as imposed by the repetition rate of the DAΦNE LINAC. Currently, PADME is operated in trigger-less mode, i.e. digitizing all channels of the detectors every single beam bunch, typically in a  $1 \mu\text{s}$  window ( $1024$  samples at  $1 \text{ Gsample/s}$ ). Of course such a system cannot be used with a continuous beam structure, so that a new trigger and DAQ system need to be designed and built.

## 2. Positron annihilation on a thick active target

**Signal signature and yield.** The cross-section for LDM production through positron annihilation on atomic electrons,  $e^+e^- \rightarrow A' \rightarrow \chi\bar{\chi}$ , is characterized by a resonant shape (20):

$$\sigma = \frac{4\pi\alpha_{EM}\alpha_D\varepsilon^2}{\sqrt{s}} \frac{q(s-4/3q^2)}{(s-m_{A'}^2)^2 + \Gamma_{A'}^2 m_{A'}^2}, \quad (3)$$

where  $s$  is the  $e^+e^-$  system invariant mass squared,  $q$  is the  $\chi - \bar{\chi}$  momentum in the CM frame, and  $\Gamma_{A'}$  is the  $A'$  width. The kinematics of the  $e^+e^- \rightarrow \chi\bar{\chi}$  reaction in the *on-shell scenario* ( $m_{A'} > 2m_\chi$ ) is strongly constrained by the underlying dynamics. Since the  $A'$  decays invisibly, its energy is not deposited in the active target, and the corresponding experimental signature is the presence of a peak in the missing energy ( $E_{miss}$ ) distribution, whose position depends solely on the  $A'$  mass through the kinematic relation

$$m_{A'} = \sqrt{2m_e E_{miss}}. \quad (4)$$

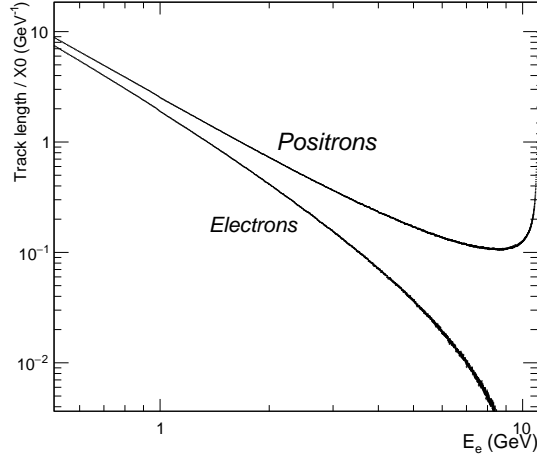


**Fig. 5.** Differential positrons track length distribution, normalized to the radiation length, for a 11 GeV  $e^+$  beam impinging on a thick target. For comparison, the same distribution in case of an impinging electron beam is reported.

For a given  $A'$  mass, the expected signal yield is:

$$N_s = n_{POT} \frac{N_A}{A} Z \rho \int_{E_{miss}^{CUT}}^{E_0} dE_e T_+(E_e) \sigma(E_e), \quad (5)$$

where  $A$ ,  $Z$ ,  $\rho$ , are, respectively, the target material atomic mass, atomic number, and mass density,  $E_0$  is the primary beam energy,  $N_A$  is Avogadro's number,  $\sigma(E_e)$  is the energy-dependent production cross-section,  $n_{POT}$  is the number of impinging positrons, and  $E_{miss}^{CUT}$  is the missing energy cut. Finally,  $T_+(E_e)$  is the positrons differential track-length distribution (21), reported in Fig. 5 for a 11 GeV positron beam.

**Positron beam requirements.** A missing energy measurement requires that the intensity of the primary positron beam is low enough so that individual  $e^+$  impinging on the active target can be distinguished. At the same time, the beam current has to be large enough to accumulate a sizeable number of positrons on target (POT). For example, a positron beam with a time structure corresponding to  $1 e^+/\mu s$  can accumulate more than  $10^{13}$  POT/year, with an average time interval between positrons of  $1 \mu s$ .

This specific time structure is challenging for the proposed CEBAF  $e^+$  operations. In particular, the low beam current,  $\sim 0.1$  pA, is incompatible with the standard beam diagnostic tools that are employed to properly steer and control the CEBAF beam. Therefore, the following “mixed operation mode” is currently being considered for the experiment (see also Fig. 6) (22). A  $10\text{-}\mu s$  long 100 nA *diagnostic macropulse* is injected in the CEBAF accelerator with a 60 Hz frequency. This results to an average current of 60 pA, with a peak current large enough to enable proper operation of the beam diagnostic systems. In between every pulse, low intensity *physics pulses*, populated *on average* by less than  $1 e^+$ , are injected at higher frequency.

This challenging operation scheme can be realized using an ad-hoc laser system at the injector. With dedicated R&D, it would be possible to design and construct a system capable

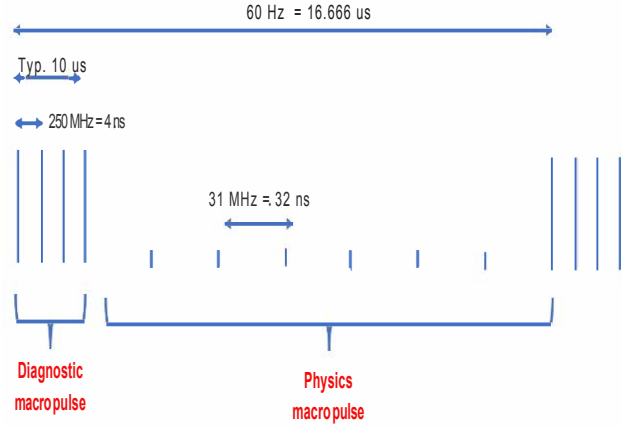


**Fig. 6.** Simplified scheme of the  $e^+$  beam time structure for the thick-target measurements, see text for details.

of injecting fast bunches at 31.25 MHz - i.e. one bunch every 32 ns. Since the (discrete) number of positrons per bunch follows a Poissonian statistical distribution, the time interval between  $e^+$  can be further increased by reducing the average bunch population, by adjusting the laser intensity. A  $\sim 500$  ns spacing between positrons can be obtained by using an average laser power of  $0.05 e^+/\text{bunch}$ . The experiment will acquire data only during low-intensity pulses, ignoring the  $10 \mu s$  long high current periods. However, if all these positrons would impact on the detector, the average rate of  $\sim 3.7 \cdot 10^8 e^+/\text{s}$  would result in a very large radiation dose deposited in the active target. To avoid this, we plan to install in front of the detector a fast magnetic deflector, synchronized to the beam 60 Hz frequency, in order to transport the positrons belonging to the high-current pulses to a suitable beam-dump, avoiding their impact on the detector.

In summary, the proposed CEBAF operation mode would allow to obtain a positron beam with particles impinging on the detector on average every  $\sim 500$  ns, compatible with the accelerator control and diagnostic system. It should be pointed out that this technical solutions requires R&D activities, that are already (partially) planned in the contest of EIC accelerator development. In the following, we will present the sensitivity to DM considering  $10^{13}$  POT accumulated in one year of run.

**Experimental setup.** The layout of the proposed measurement is schematically reported in Fig. 7. It includes a homogeneous electromagnetic calorimeter (ECAL) acting as a thick target to measure the energy of each impinging positron, and a hadron detection system (HCAL) installed around and downstream the active target to measure long-lived (neutrons/ $K_L$ ) or highly penetration (muons/charged pions) particles escaping from the ECAL.

The *preliminary* ECAL design foresees a 28 radiation lengths detector, made as a  $10 \times 10$  matrix of  $20 \times 20 \times 250 \text{ mm}^3$   $\text{PbWO}_4$  crystals. Three layers of crystals are added in front, with the long axis oriented perpendicular to the beam direction, to act as a pre-shower, resulting in a total calorimeter length of  $35 X_0$ . The choice of  $\text{PbWO}_4$  material is motivated by its fast

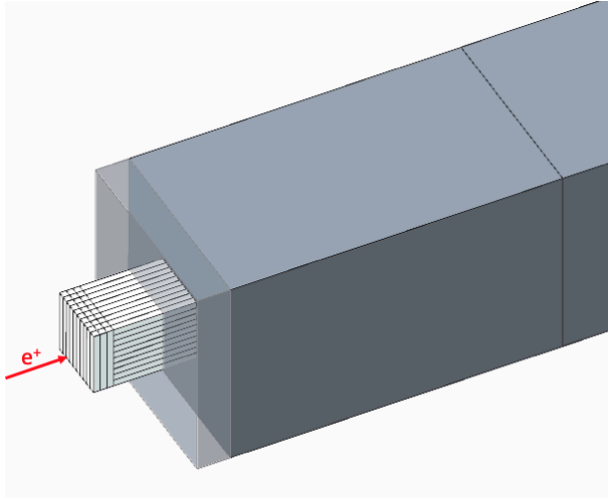


**Fig. 7.** Schematic layout of the active thick-target experimental setup, with the ECAL (white) followed and surrounded by the HCAL (gray). The semi-transparent portion of the HCAL in front is that installed all around the ECAL.

scintillating time ( $\tau \simeq 30$  ns), well matched to the expected hit rate, its high-density, resulting in a compact detector, and its high radiation hardness. The total calorimeter length was selected to limit below  $\sim 10^{-13}$  per POT the probability that any particle from the developing cascade, in particularly photons, escape the detector faking a signal. The transverse size, was chosen to provide measurements of the shower transverse profile and to optimize the optical matching with the light sensor. The total front face size ( $20 \times 20$  cm<sup>2</sup>) is large enough to avoid transverse energy leakage affecting the detector resolution. Silicon Photomultipliers will be used to collect scintillation light from the crystals. The use of these sensors has never been adopted so far in high-energy electromagnetic calorimetry with PbWO<sub>4</sub> crystals, and requires a careful selection of the corresponding parameters. First measurements on PbWO<sub>4</sub> crystals with  $6 \times 6$  mm<sup>2</sup> devices having a  $25$   $\mu$ m pixel size show a light yield of  $\sim 1$  phe / MeV, compatible with the experiment requirements (energy resolution and dynamic range). The expected radiation dose for the detector, for positrons impinging on the calorimeter every 500 ns and assuming an overall beam availability of 50% is, at maximum,  $\sim 350$  rad/h, corresponding to the central crystals. This large value, comparable to the maximum dose in the CMS PbWO<sub>4</sub> electromagnetic calorimeter (23, 24), calls for a careful calorimeter design and for the identification of procedures to mitigate any possible radiation damage during detector operation. These include varying the beam impact point on the detector to distribute the radiation dose across crystals, as well as annealing crystals during no-beam operations, exploiting both thermal annealing and light-induced processes (25, 26).

The main requirement for the HCAL is the hermeticity to long-lived particles exiting from the ECAL. From a Monte-carlo simulation of this setup, the probability of having one or more high-energy ( $\gtrsim 1$  GeV) hadron leaving the active target is  $\sim 10^{-4}$  per POT. This calls for a HCAL inefficiency of  $10^{-10}$  or lower. The *preliminary* detector design uses a modular iron/scintillator inhomogeneous calorimeter, with

a length corresponding to approximately 25 nuclear interaction lengths, partially surrounding the active target to avoid any particle leakage from the calorimeter lateral faces.

**Measurement and analysis strategy.** The experiment will be characterized by a very high measurement rate, dominated by events with full energy deposition in the calorimeter. To cope with this, the data acquisition system will be configured to record only events with a significant ( $\gtrsim 1$  GeV) energy loss in the calorimeter. From a preliminary estimate, the expected trigger rate will be  $\sim 20$  kHz, for a primary beam impinging with 2 MHz frequency on the detector. This minimum bias condition will be initially studied with Monte-carlo simulations, to evaluate the efficiency and confirm that no distortions to the experiment physics outcome are introduced. In parallel to the main production trigger, prescaled trigger conditions will be implemented to save full-energy events for calibration and monitoring.

A blind approach to data analysis will be followed. First, events in the signal region, based on a preliminary choice of the calorimeter and hadron detection system energy cuts, will be excluded from the analysis. Then, the expected number of backgrounds will be evaluated using both Monte-carlo simulations and events in the neighborhood of the signal region, in order to identify an optimal set of selection cuts for the signal that maximize the experiment sensitivity (27). Finally, the signal region will be scrutinized.

## Results

The sensitivity of the two proposed measurements is shown in Fig. 8, compared with current exclusion limits (gray areas) and expected performance of other missing-energy / missing-mass future experiments (dashed curves). On the same plot, we show the thermal targets for significant variations of the minimal LDM model presented in the introduction: elastic and inelastic scalar LDM (I), Majorana fermion LDM (II), and pseudo-Dirac fermion LDM (III). For the thin-target effort, the red curve reports the sensitivity estimate based on the realistic backgrounds that have been discussed before. For the thick-target case, the orange curve refers to the ideal case of a zero-background measurement. This hypothesis, following what was done in similar experiments (28, 29), will be investigated with Monte-carlo simulations during the future experiment design phase.

**Complementarity of the two approaches.** The two measurements that we presented in this document are characterized by a different sensitivities and design complexity. They can be considered as two complementary experiments facing the light dark matter physical problem, and as such we foresee a comprehensive LDM physical program at JLab with both of them running, but with different time schedules.

With the availability of a 100 nA, 11 GeV positron beam at JLab, the thin-target experiment can start almost immediately, since no demanding requirements on the beam are present. The conceptual design is already mature, being based on realistic Monte-carlo simulations. Furthermore, the



## Supplementary Note 1: Full list of authors and affiliations

R. Henriques<sup>a</sup>, R. Henriques<sup>b</sup>, R. Henriques<sup>c</sup>, R. Henriques<sup>d</sup>, R. Henriques<sup>e</sup>, R. Henriques<sup>f</sup>, R. Henriques<sup>g</sup>, R. Henriques<sup>h</sup>, R. Henriques<sup>i</sup>

<sup>a</sup>*MRC Laboratory for Molecular Cell Biology and Department of Cell and Developmental Biology  
University College London, Gower Street, London, WC1E 6BT, United Kingdom*

<sup>b</sup>*MRC Laboratory for Molecular Cell Biology and Department of Cell and Developmental Biology  
University College London, Gower Street, London, WC1E 6BT, United Kingdom*

<sup>c</sup>*MRC Laboratory for Molecular Cell Biology and Department of Cell and Developmental Biology  
University College London, Gower Street, London, WC1E 6BT, United Kingdom*

<sup>d</sup>*MRC Laboratory for Molecular Cell Biology and Department of Cell and Developmental Biology  
University College London, Gower Street, London, WC1E 6BT, United Kingdom*

<sup>e</sup>*MRC Laboratory for Molecular Cell Biology and Department of Cell and Developmental Biology  
University College London, Gower Street, London, WC1E 6BT, United Kingdom*

<sup>f</sup>*MRC Laboratory for Molecular Cell Biology and Department of Cell and Developmental Biology  
University College London, Gower Street, London, WC1E 6BT, United Kingdom*

<sup>g</sup>*MRC Laboratory for Molecular Cell Biology and Department of Cell and Developmental Biology  
University College London, Gower Street, London, WC1E 6BT, United Kingdom*

<sup>h</sup>*MRC Laboratory for Molecular Cell Biology and Department of Cell and Developmental Biology  
University College London, Gower Street, London, WC1E 6BT, United Kingdom*

<sup>i</sup>*MRC Laboratory for Molecular Cell Biology and Department of Cell and Developmental Biology  
University College London, Gower Street, London, WC1E 6BT, United Kingdom*